



저작자표시-비영리-변경금지 2.0 대한민국

이용자는 아래의 조건을 따르는 경우에 한하여 자유롭게

- 이 저작물을 복제, 배포, 전송, 전시, 공연 및 방송할 수 있습니다.

다음과 같은 조건을 따라야 합니다:



저작자표시. 귀하는 원저작자를 표시하여야 합니다.



비영리. 귀하는 이 저작물을 영리 목적으로 이용할 수 없습니다.



변경금지. 귀하는 이 저작물을 개작, 변형 또는 가공할 수 없습니다.

- 귀하는, 이 저작물의 재이용이나 배포의 경우, 이 저작물에 적용된 이용허락조건을 명확하게 나타내어야 합니다.
- 저작권자로부터 별도의 허가를 받으면 이러한 조건들은 적용되지 않습니다.

저작권법에 따른 이용자의 권리는 위의 내용에 의하여 영향을 받지 않습니다.

이것은 [이용허락규약\(Legal Code\)](#)을 이해하기 쉽게 요약한 것입니다.

[Disclaimer](#)

Master's Thesis

Polyethylenimine aerogels for catalyst-free  
electrochemical hydrogen production

Misol Bae

School of Energy and Chemical Engineering  
(Energy Engineering)

Ulsan National Institute of Science and Technology

2022

# Polyethylenimine aerogels for catalyst-free electrochemical hydrogen production

Misol Bae

School of Energy and Chemical Engineering  
(Energy Engineering)

Ulsan National Institute of Science and Technology

# Polyethylenimine aerogels for catalyst-free electrochemical hydrogen production

A thesis/dissertation submitted to  
Ulsan National Institute of Science and Technology  
in partial fulfillment of the  
requirements for the degree of  
Master of Science

Misol Bae

01.10.2022 of submission

Approved by

---

Advisor

Jungki Ryu

# Polyethylenimine aerogels for catalyst-free electrochemical hydrogen production

Misol Bae

This certifies that the thesis/dissertation of Misol Bae is approved.

01.10.2022 of submission

Signature

---

Advisor: Jungki Ryu

Signature

---

Ji-Wook Jang

Signature

---

Dong Woog Lee

Signature

## Abstract

In a crisis of climate change and environmental pollutions, many researchers have been interested in so-called green hydrogen fuel through water-splitting since it can be generated from surplus renewable electricity and carried into a grid by chemical energy conversion. To make water splitting feasible, most studies have focused on synthesizing cost-effective electrocatalysts. However, the removal of gas bubbles from the electrode surface is a practically important issue to maintain the activity of electrochemical gas evolution reactions and less attention has been paid to the bubble removal issues. Recently, it is reported that the adhered gas bubbles can be readily eliminated by imparting extremely gas-repellent properties (so-called superaerophobicity) to electrodes via controlling their nano/microstructure based on the Cassie-Baxter wettability model. Unfortunately, this approach is material-specific and requires harsh and expensive synthetic conditions, making it difficult to scale up. To address these issues, we report a universal method to impart superaerophobicity to various electrodes such as Ni foam and Pt (FTO) through simple coating with cheap polymer-polyethylenimine (PEI, Mn=10000)-aerogel without affecting underlying target substrates. From catalyst-free aerogel modification, as-generated gas bubbles can be easily removed from the surface of electrodes, leading to enhanced hydrogen production performance comparable to other electrocatalysts. This approach can be applied to dealing with the impeded mass transfer ascribed to adhesive bubbles and provides insights for designing various energy conversion devices such as commercialized water electrolyzers.



## Contents

<b>List of Figures</b> .....	
<b>List of Tables</b> .....	
<b>Nomenclature</b> .....	
<b>1 Introduction</b> .....	
1.1 Research Background .....	1
1.2 Water Splitting .....	2
1.3 Superaerophobicity .....	3
1.4 Distinction of Our Research .....	4
<b>2 Experimental Section</b> .....	5
<b>3 Results and Discussion</b> .....	
3.1 Research Overview .....	7
3.2 Characterizations .....	8
3.3 Analysis of Wettability .....	10
3.4 Electrochemical Activities .....	16
<b>Conclusion</b> .....	23
<b>References</b> .....	24

## List of Figures

**Figure 1.** The energy flow of hydrogen fuel via water splitting by using renewable electricity.

**Figure 2.** The general process of water splitting.

**Figure 3.** The diameter of adhered bubbles during growing and releasing periods depending on wettability.

**Figure 4.** Underlying the mechanism of bubbles dissipation (a) without aerogel modification, (b) with aerogel modification. To be specific,  $F_b = \frac{4}{3}\pi r^3 \Delta\rho g$  (eq. 3) and  $F_s = -2\pi r \gamma \sin^2\theta$  (eq. 4), where  $r$  is a radius of the bubble,  $\Delta\rho$  is a density difference between the electrolyte and gas bubble,  $g$  is the gravitational acceleration,  $\gamma$  is the intrinsic surface tension of electrolyte, and  $\theta$  is an angle between the electrolyte and electrode surface.

**Figure 5.** (a) The illustrated comparison with viscous mixture and aerogels after freeze-drying. (b) SEM image of bare Ni foam and inset image is a photograph of pristine Ni foam. (c) SEM image of deposited PEI aerogel on Ni foam and an inset shows a photograph of aerogel modified porous electrode. (d) SEM image of bare FTO coated with Pt (Pt (FTO)) and inset photograph indicates pristine Pt (FTO). (e) SEM image of PEI cross-linked layer on Pt (FTO) and inset picture shows aerogel modified flat electrode. All the substrates were pre-treated with APTES, and the concentration of PEI was 2%.

**Figure 6.** Fourier-transform infrared (FT-IR) spectroscopy of PEI 2% polymer and PEI 2% aerogel.

**Figure 7.** (a) The HER effect of aerogels deposited on Ni foams depending on PEI concentrations. (All the substrates were coated with APTES treatment.) (b) The correlation between the air contact angles, porosity, and applied voltages based on (a) at  $-500 \text{ mA/cm}^2$ . (c) The comparison of bare Ni foam and PEI 2% aerogel on NF, (d) pristine flat Pt, and PEI 2% aerogel on Pt depending on an iR correction (85%).

**Figure 8.** The measured air contact angles on Si wafers. All aerogels were coated on APTES treated Si wafers.

**Figure 9.** The HER effect of APTES treatment on target electrodes in 1M KOH. Solid lines mean the pristine electrodes without treatment, and dot lines indicate APTES treated electrodes.

**Figure 10.** The measured air contact angles of PEI 2% aerogels on Ni foam and Pt (FTO). (All the substrates were coated with APTES treatment.)

**Figure 11.** SEM images of porous structures with different concentrations of PEI aerogels deposited on Ni foams with APTES treatments.

**Figure 12.** The correlations between pore's size and porosity depending on PEI concentrations from Figure 11. (PEI-0.5% didn't form the aerogel, so we excluded it for calculations.)

**Figure 13.** (a) The HER effect of Ru layer depending on an iR correction, and (b) the relationship between corresponding discrepancy in applied voltage at  $-500\text{mA}/\text{cm}^2$  (w/ and w/o iR corrections) and air contact angles.

**Figure 14.** (a) The HER performance of PEI 2% aerogel deposited on Ni foam and other electrocatalysts without iR corrections. (b) The corresponding Tafel comparison from (a). (c) The EIS analysis of porous Ni foams related to (a). (d) The corresponding bar graph of (c) EIS analysis. (All the target substrates for coating aerogels were pretreated with APTES.)

**Figure 15.** SEM images of alkaline electrocatalysts, (a)  $\text{Ni}(\text{OH})_2$ , (b)  $\text{FeNi}@/\text{FeNi}$ , (c) NTA, and (d) Ru layer.

**Figure 16.** The bar graph corresponding to Figure 3a.

**Figure 17.** (a) The EIS analysis of bare NF and PEI 2% aerogel. (b) The EIS of the flat model and (c) corresponding bare graph.

**Figure 18.** (a) The ECSA of bare Ni foam and PEI 2% aerogel on Ni foam. (b) The ECSA of flat Pt model. (Scan rate with 10/30/70/130/210/310 mV/s.)

**Figure 19.** (a) Chronopotentiometry at  $-10\text{ mA}/\text{cm}^2$  for 12hr with 350 rpm of the aerogel deposited on Ni foam vs. bare Ni foam. (b) Measurement of LSV after the cyclic voltammetry (CV) 1000 times within the same sweep potential range. (c) Raman shift to confirm the functional groups after long-term stability tests. (d) SEM images after A: (a)/B: (b) stability tests, respectively.

## **List of Tables**

**Table 1.** The EIS of (a) a porous system and the EIS of (b) a flat system.

## Nomenclature

---

<b>RE</b>	Renewable energy
<b>CEC</b>	Chemical energy conversion
<b>CCS</b>	Carbon capture and storage
<b>HER</b>	Hydrogen evolution reaction
<b>OER</b>	Oxygen evolution reaction
<b>PEI</b>	Polyethylenimine
<b>SEM</b>	Scanning electron microscopy
<b>Pt (FTO)</b>	Platinum coated on fluorine-doped tin oxide
<b>FT-IR</b>	Fourier-transform infrared spectroscopy
<b>LSV</b>	Linear sweep voltammetry
<b>APTES</b>	(3-Aminopropyl)triethoxysilane
<b>KOH</b>	Potassium hydroxide
<b>EIS</b>	Electrochemical impedance spectroscopy
<b>ECSA</b>	Electrochemical surface area
<b>CV</b>	Cyclic voltammetry

---

# 1. Introduction

## 1.1 Research Background

In a crisis of climate change and severe environmental problems, the importance of developing renewable energy (RE) is getting rising. To satisfy the increasing demand for clean and sustainable energy, numerous studies have focused on generating electricity without emitting pollutants such as carbon dioxide. However, renowned alternate energy systems such as wind, solar or tidal power are operated intermittently within restricted continental locations and depending on the weather condition. On the other hand, hydrogen energy is taking a more and more important role in RE, because it can be carried into a grid by chemical energy conversion (CEC) (**Figure 1**).<sup>1, 2</sup> There are three types of producing hydrogen. First, Grey hydrogen: split natural gas into hydrogen and CO<sub>2</sub> without carbon capture and storage (CCS). Second, Blue hydrogen: like producing grey hydrogen, but adding CCS process. The last: Green hydrogen: producing hydrogen by water splitting, and it doesn't emit CO<sub>2</sub>. Therefore, among three categories, an authentic sustainable alternative energy is considered green hydrogen and the green hydrogen fuel can be generated from the existing intermittent electricity.

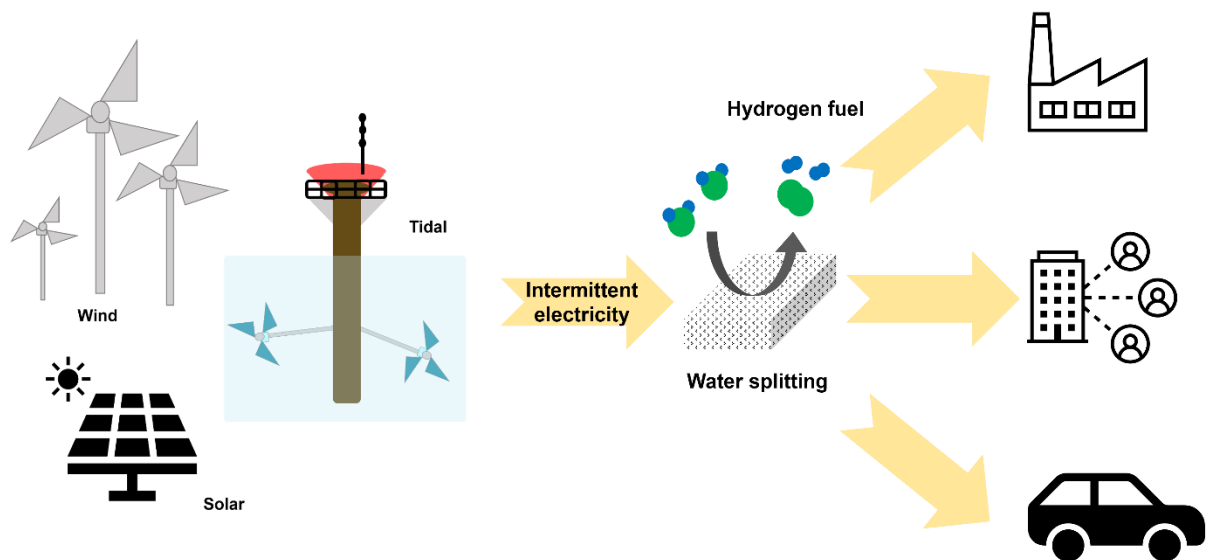


**Figure 1.** The energy flow of hydrogen fuel via water splitting by using renewable electricity.

## 1.2 Water Splitting

Since the water splitting process is a redox couple, generally hydrogen and oxygen gas are produced at cathode (reduction) and anode (oxidation), respectively (**Eq. 1**) (**Figure 2**).<sup>3</sup>

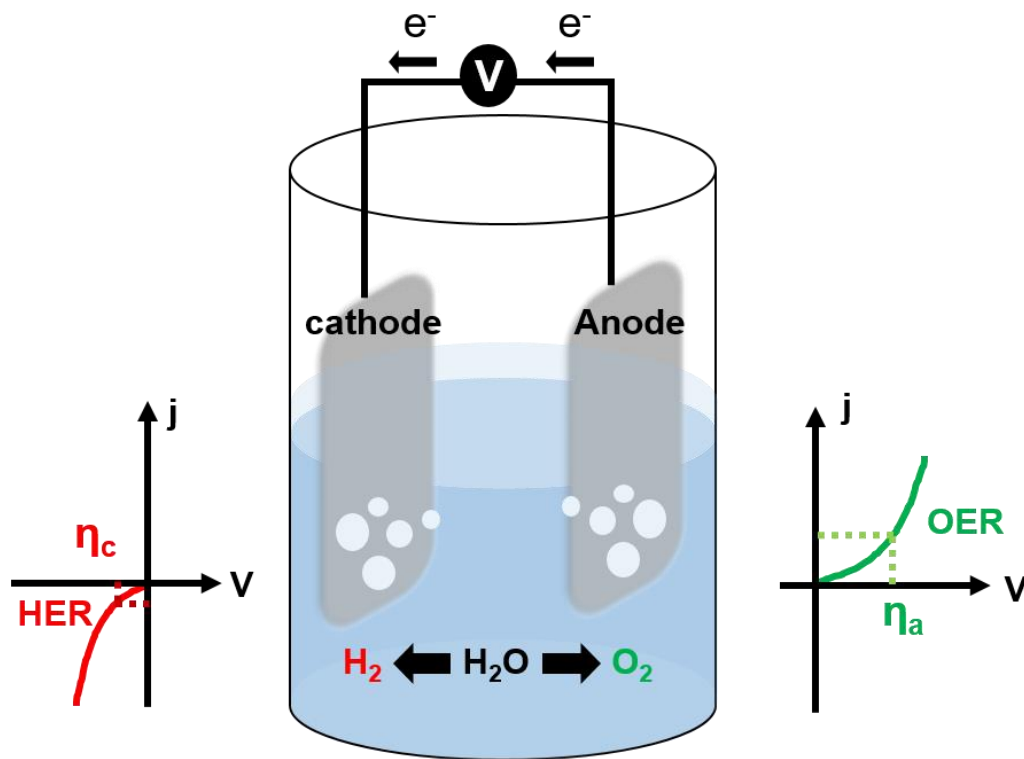
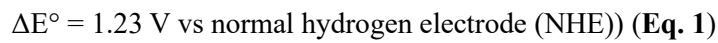
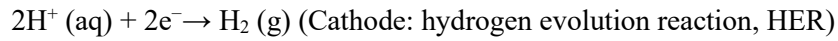
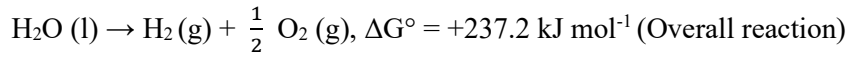


**Figure 2.** The general process of water splitting.

However, the actual energy requires more than the theoretical value ( $\Delta E^\circ = 1.23 \text{ V}$ ) to overcome the activation energy called overpotential ( $\eta$ ). Therefore, much research has attempted to minimize the overpotential ( $\eta$ ) by devising a cost-effective catalytic system in both HER and OER.

### 1.3 Superaerophobicity

On the other hand, the adsorption and desorption of gas bubbles during water splitting have been overlooked despite their practical importance. The adhered bubbles can block the electrochemically active sites of electrodes/catalysts and impede mass transport, substantially increasing overpotentials.<sup>4</sup> Generally, the as-generated gas bubbles grow until the buoyancy force  $F_b$  (Eq. 3) overcomes the surface tension force  $F_s$  (Eq. 4) (Figure 3).<sup>5</sup> Then the gas bubbles can continuously exert stretch force ( $\partial_f$ ) to the electrode/catalysts upon their desorption, causing the degradation and even exfoliation of catalysts.<sup>6-8</sup> Therefore, these issues can lower the overall efficiency of producing hydrogen fuel through water-splitting even with excellent electrocatalysts.<sup>9</sup>

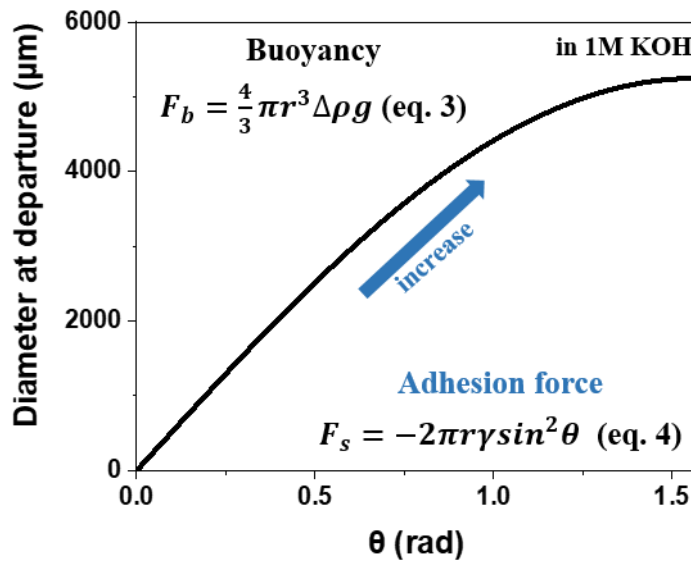


**Figure 3.** The diameter of adhered bubbles during growing and releasing periods depending on wettability.

To address these issues, researchers developed a strategy to impart bubble-repellent properties to electrodes/catalysts by controlling their morphology.<sup>10, 11</sup> For example, researchers reported the fabrication of an extremely gas bubble-repellent electrode with a gas bubble contact angle of  $>150^\circ$  (i.e., superaerophobic) by vertically aligning  $\text{MoS}_2$  nanoplatelets and making arrays of  $\text{RuO}_2/\text{TiO}_2$  nanosheet.<sup>4-6, 10-14</sup> They found that the superaerophobic film can facilitate the gas removal and greatly improve the efficiency of various gas evolution reactions, including hydrogen evolution reaction (HER). According to the Cassie-Baxter model, hydrophilic nano/microstructured substrates can be more exposed to the electrolyte and eliminate gas bubbles more efficiently than the flat counterpart.<sup>15-17</sup> However, such strategies of directly controlling the nano/microstructure of electrodes and catalysts can

have limitations for practical application. They require the development of material-specific synthesis methods often under harsh conditions, making them difficult to scale up.

#### **1.4 Distinction of Our Research**

In our previous research, the superaerophobic M13 virus overlayer had a limitation of multiplying the virus, and it was hard to apply in practical use due to less feasibility of scale-up.<sup>18</sup> In this study, we report a simple strategy to fabricate superaerophobic electrodes via coating with polyethylenimine (PEI) aerogel for efficient and stable hydrogen production even without HER catalysts. Aerogels were coated on target substrates, such as flat Pt film and microporous Ni foam, by crosslinking inexpensive PEI via Schiff-base condensation reactions followed by freeze-drying. We can readily control the pore size, porosity, and superaerophobicity of PEI aerogel by varying the concentrations of PEI upon crosslinking. We demonstrated that the deposition of hierarchically porous PEI aerogels substantially improves that the HER performance of the flat Pt and Ni foam electrode without significant performance degradation for 12 h. At high current densities, the Ni foam modified with the PEI aerogel exhibited a superior performance even without HER electrocatalysts, such as Ni(OH)<sub>2</sub>, NTA, FeNi@FeNi, and Ru layer due to a notable decrease of the series resistance related to ionic conductance. These results suggest the universal applicability of our approach for enhanced hydrogen evolution by controlling the wettability of electrodes with cheap polymer-based aerogels.

## 2. Experimental sections

### Materials.

Nickel foam (thickness: 1.6mm) was purchased from MTI (Korea). Pt film (100-nm) was coated on Fluorine-doped tin oxide (FTO, averaged thickness: 500nm and 7 ohm) by an e-beam evaporator. Polyethylenimine (PEI, Mn= 10000 with d= 1.03 g/ml), KOH ( $\geq 85\%$ ), HCl (37%), NaCl, (3-aminopropyl)triethoxysilane (99 %), and ethanol were purchased from Sigma-Aldrich Aldrich (USA). Glutaraldehyde (50wt% in H<sub>2</sub>O) was obtained from Alfa Aesar (USA).

### Preparation of Polyethylenimine (PEI) solutions.

PEI 2% (v/v) solution was prepared by diluting PEI polymer with D.I water, specifically, mixing 25.75 mg/ml of PEI with 37.5 mM NaCl on basis of 0.27 M HCl to adjust to the pH around D.I water. The PEI concentrations of gel-0.5%, gel-5.5%, and gel-7.3% were 5.14 mg/ml, 59.49 mg/ml, and 80.51 mg/ml, respectively (with different HCl concentrations).

### APTES Treatment of electrodes.

Before the deposition of PEI aerogels, all substrates were followed by the APTES coating process according to the literature for better adhesion with electrodes.<sup>19</sup>

### Coating PEI aerogels on Ni foam/ Pt (FTO).

PEI aerogels were coated on Ni foam by dipping it in PEI 2% solution with mild stirring for 1 hour and followed by baking it at 120°C for 10 min for better linking to APTES functional groups.<sup>20, 21</sup> After baking, PEI-coated Ni foam was dipped into 1wt% glutaraldehyde (in H<sub>2</sub>O) for 1 min and freeze-dried. The PEI aerogel layer was deposited on Pt (FTO) by spin-coating (1250rpm, 2min) and followed the same fabrication procedure with Ni foam, but it was dipped to 1wt% glutaraldehyde for 5min.

### Preparation of alkaline electrocatalysts.

The synthetic procedures were followed by works of literature, Ni(OH)<sub>2</sub> nanoparticles,<sup>22</sup> FeNi@FeNi,<sup>23</sup> Nickel nanotube array (NTA),<sup>24</sup> and Ru layer,<sup>25</sup> respectively.

### Preparation of samples for measuring contact angles.

Different concentrations of PEI aerogels were coated on Si wafers with APTES treatment by doctor blading through the same volume of PEI and GA.

### **Characterization.**

Morphology of aerogels was investigated by a scanning electron microscope (SEM) (Hitachi S-4800, Japan). Averaged pore diameter and porosity of aerogels were calculated using the home-made analyzer. The air-contact angles were measured by a DSA100 drop shape analysis (DSA100, Germany). Fourier-transform infrared (FT-IR) spectroscopy was performed with a ATR mode (Agilent, USA). Raman spectroscopy (alpha300S, Germany) was examined at  $532\text{nm}^{-1}$ .

### **Electrochemical measurements.**

All electrochemical characterizations were conducted in 1M KOH (pH= 14). All pristine electrodes were treated with APTES treatment, except synthesizing the alkaline electrocatalysts. Polarization curves were measured by using an SP-150 potentiostat/galvanostat (Bio-Logic Science Instruments, France) under the following conditions: a reference electrode, Ag/AgCl (1M KCl saturated); a counter electrode, Pt mesh; and scan rate, 10 mV/s. Electrochemical impedance spectra were measured under the following conditions: a reference electrode, Ag/AgCl; a counter electrode, Pt mesh; applied potential,  $-0.25\text{ V}$  vs. RHE for a porous model and  $-50\text{mA}/\text{cm}^2$  for a flat model; amplitude, 20 mV; and frequency scan range, 100 kHz to 0.1 Hz.

### 3. Result and Discussion

#### 3.1 Research Overview

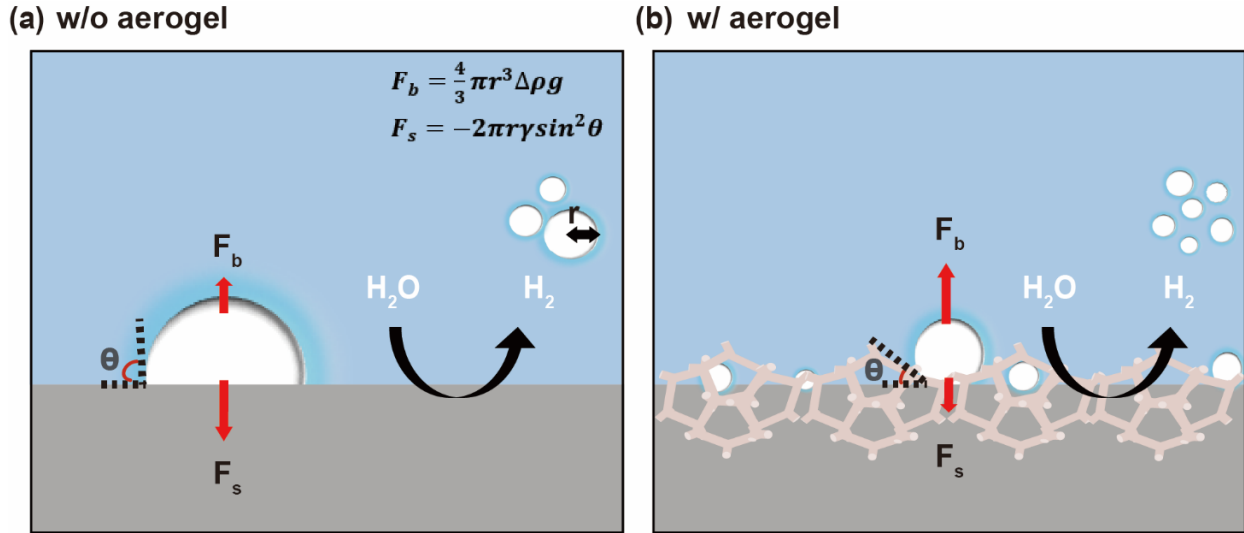


**Figure 4.** Underlying the mechanism of bubbles dissipation (a) without aerogel modification, (b) with aerogel modification. To be specific,  $F_b = \frac{4}{3}\pi r^3 \Delta\rho g$  (eq. 3) and  $F_s = -2\pi r\gamma \sin^2\theta$  (eq. 4), where  $r$  is a radius of the bubble,  $\Delta\rho$  is a density difference between the electrolyte and gas bubble,  $g$  is the gravitational acceleration,  $\gamma$  is the intrinsic surface tension of electrolyte, and  $\theta$  is an angle between the electrolyte and electrode surface.

We hypothesized that the HER efficiency could be enhanced through bubble-repellent property induced by coating hydrophilic aerogels on target substrates. To be specific, the surface tension force (eq. 4) from the superaerophobic electrodes ( $\theta$  is under  $30^\circ$ ) could be weaker than the buoyancy (eq. 3) within the same volume of hydrogen bubbles, and the bubbles were faster dissipated without holding on growth (Figure 4).<sup>7</sup> In this work, we triggered the superaerophobicity from the PEI aerogel by using glutaraldehyde (GA) kept in constant 1wt% as a cross-linker. We utilized the cationic polymer, branched PEI ( $M_n = 10000$ ) as a building framework, due to its low cost, hydrophilicity, and abundant  $\text{NH}_2$  groups for crosslinking.<sup>26</sup> We expected that the aerogel had a low surface tension force due to the superaerophobicity, improved the access of the ions from the electrolyte to electrodes, and thus facilitated hydrogen production. Additionally, the fabrication of the catalyst-free aerogels can be regarded simple and cost-effective rather than other catalytic modifications.

### 3.2 Characterizations

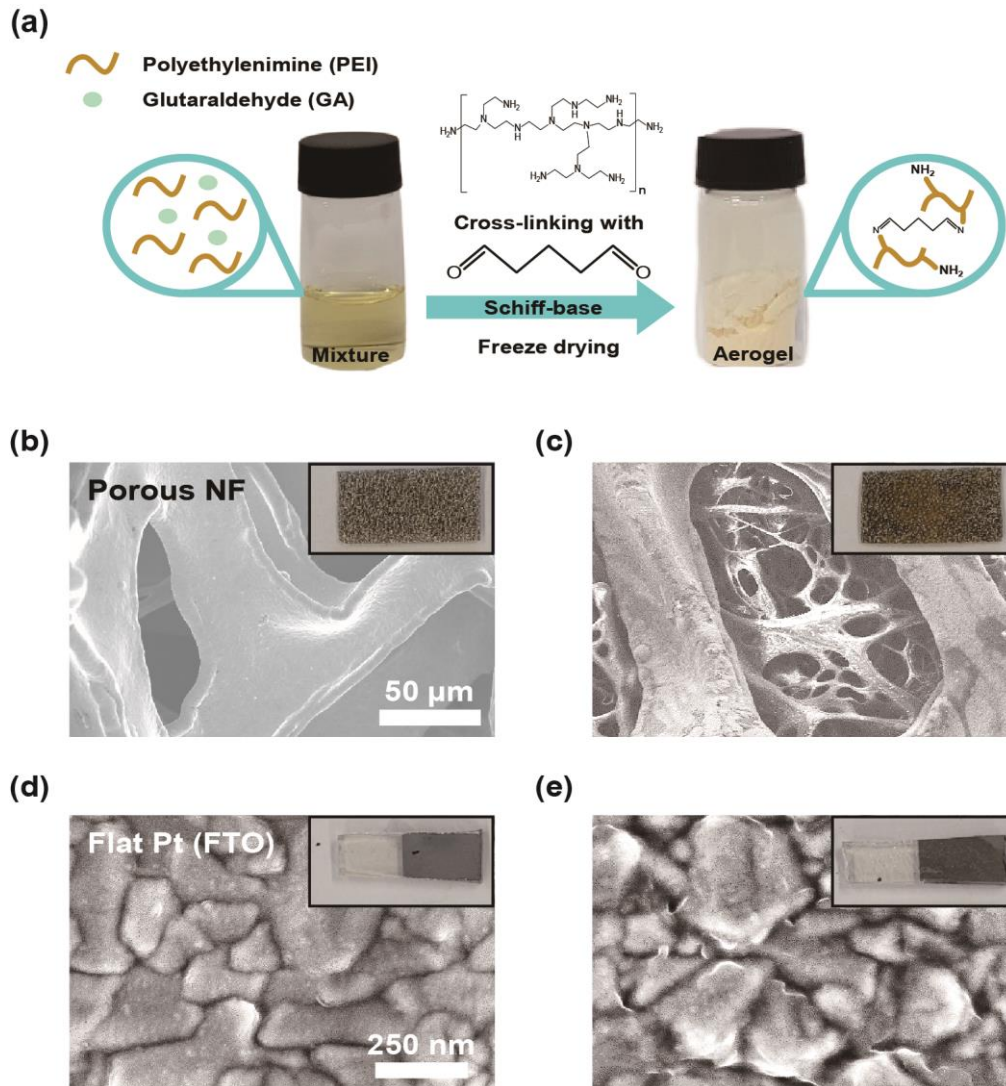


**Figure 5.** (a) The illustrated comparison with viscous mixture and aerogels after freeze-drying. (b) SEM image of bare Ni foam and inset image is a photograph of pristine Ni foam. (c) SEM image of deposited PEI aerogel on Ni foam and an inset shows a photograph of aerogel modified porous electrode. (d) SEM image of bare FTO coated with Pt (Pt (FTO)) and inset photograph indicates pristine Pt (FTO). (e) SEM image of PEI cross-linked layer on Pt (FTO) and inset picture shows aerogel modified flat electrode. All the substrates were pre-treated with APTES, and the concentration of PEI was 2%.

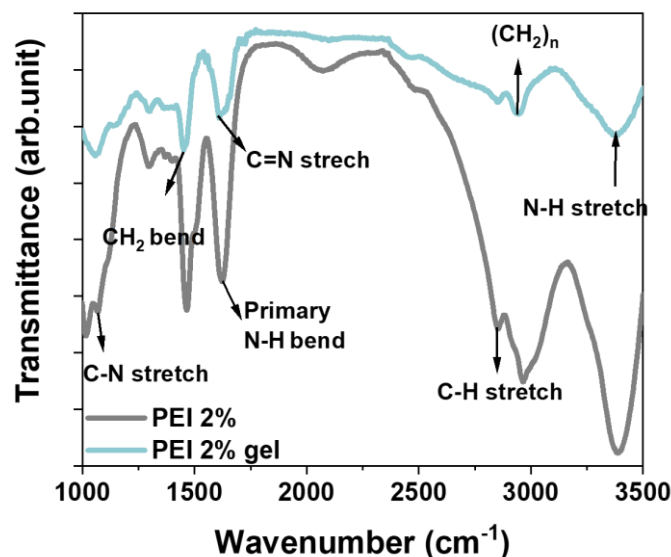


**Figure 6.** Fourier-transform infrared (FT-IR) spectroscopy of PEI 2% polymer and PEI 2% aerogel.

First, we confirmed the formation of aerogels on target substrates (**Figure 5**). When diluted PEI solution was mixed with the same volume of GA (**Figure 5a**), the mixture turned colorless into the viscous yellow liquid. After freeze-drying, all the liquid entities were evaporated, and only densely cross-linked aerogels remained under the Schiff-base reaction.<sup>27</sup> The morphology of the deposited aerogels was investigated through scanning electron microscopy (SEM) (**Figure 5 b to e**). We observed the coating of aerogels on each target electrode independent of the morphology of underlying substrates. To guarantee cross-linking of PEI with GA, we confirmed the structure of uncross-linked PEI 2% and PEI 2% aerogel by Fourier-transform infrared (FT-IR) spectroscopy (**Figure 6**). N-H stretches were commonly observed from both the uncross-linked PEI 2% polymer and PEI 2% aerogel at  $3383\text{ cm}^{-1}$ . Among a range of  $3000\text{--}2840\text{ cm}^{-1}$  for C-H stretches, the distinct peak at  $2941\text{ cm}^{-1}$  on aerogel was assigned to  $(\text{CH}_2)_n$  under cross-linking with GA. The uncross-linked polymer had a dominant peak at  $1623\text{ cm}^{-1}$ , indicating the N-H bend from a primary amine, whereas aerogel had C=N from PEI cross-linked with GA at  $1610\text{ cm}^{-1}$  by the Schiff-base reaction. The bands ( $1465, 1450\text{ cm}^{-1}$ ) and  $1070\text{ cm}^{-1}$  were C-H bend and C-N stretch, respectively.<sup>28-30</sup> These results support the deposition of porous aerogels on target substrates by cross-linked PEI followed by freeze-drying.

### 3.3 Analysis of Wettability

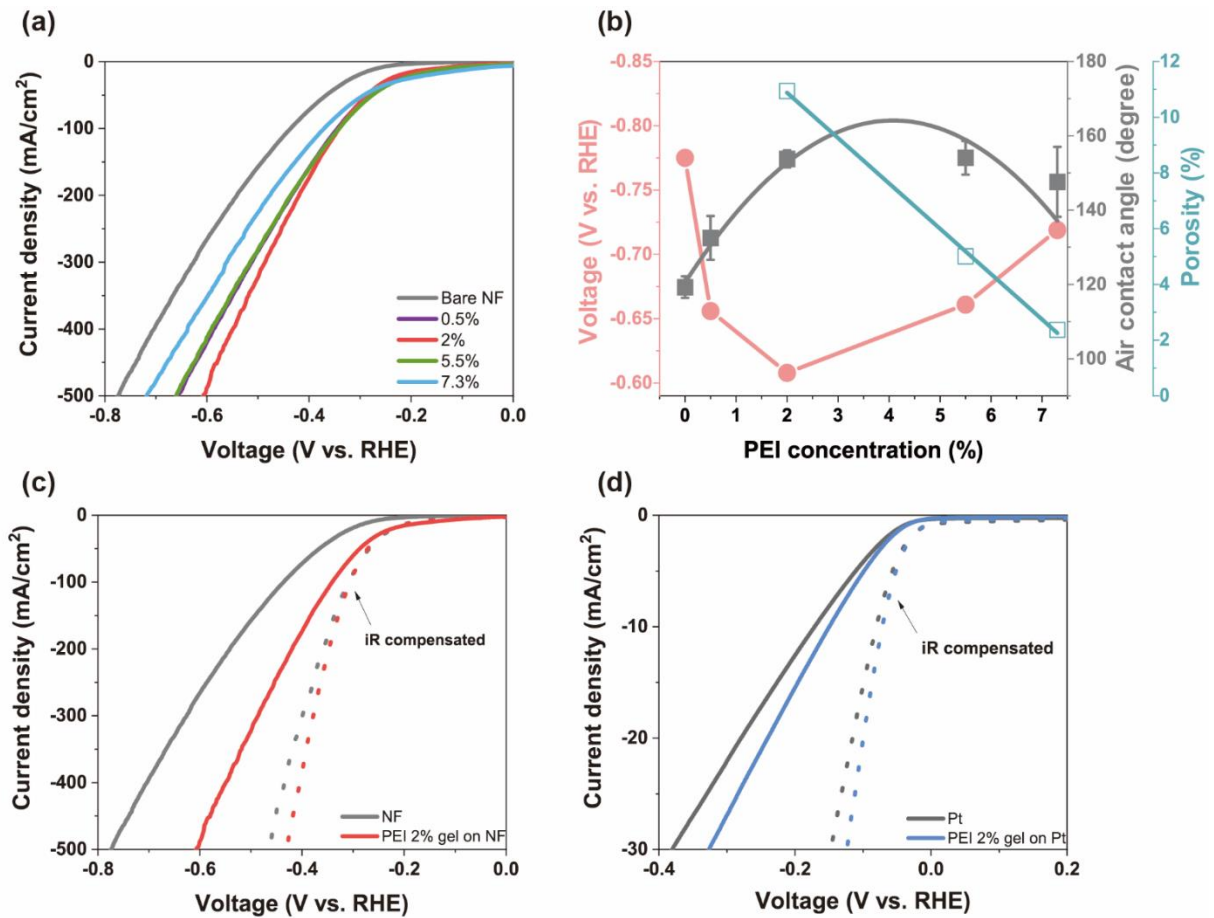


**Figure 7.** (a) The HER effect of aerogels deposited on Ni foams depending on PEI concentrations. (All the substrates were coated with APTES treatment.) (b) The correlation between the air contact angles, porosity, and applied voltages based on (a) at  $-500 \text{ mA}/\text{cm}^2$ . (c) The comparison of bare Ni foam and PEI 2% aerogel on NF, (d) pristine flat Pt, and PEI 2% aerogel on Pt depending on an iR correction (85%).

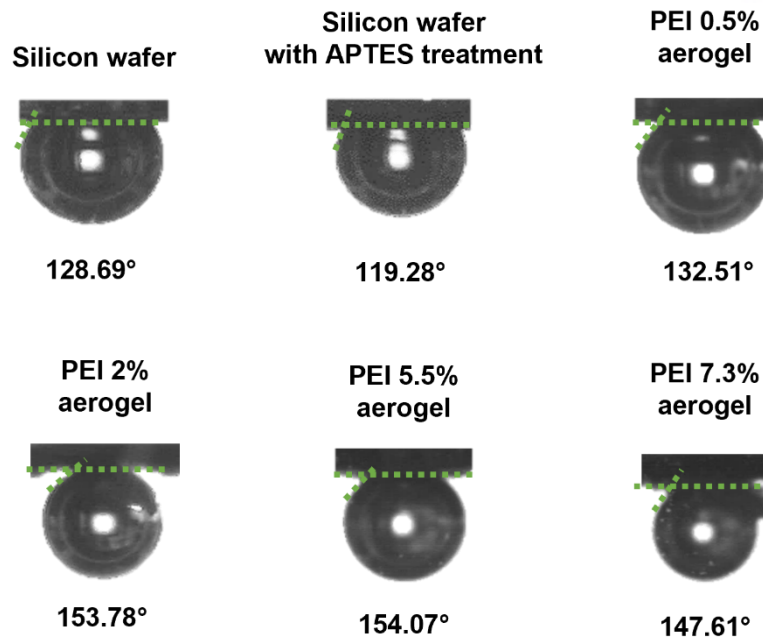


**Figure 8.** The measured air contact angles on Si wafers. All aerogels were coated on APTES treated Si wafers.

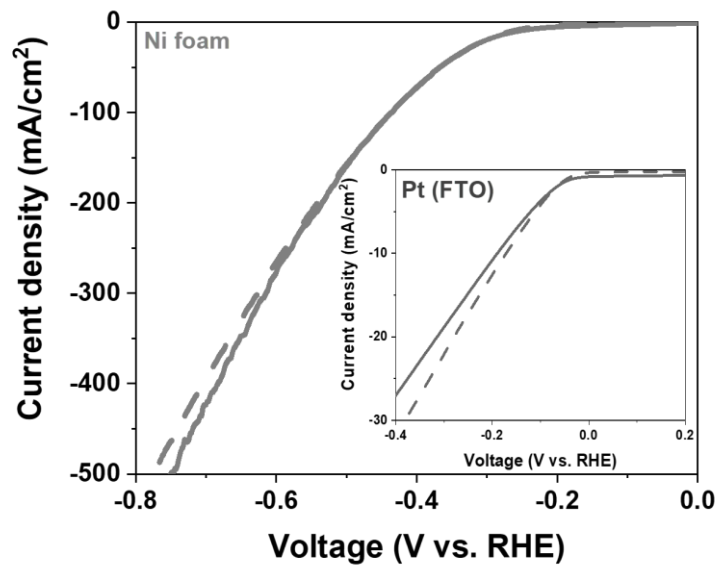


**Figure 9.** The HER effect of APTES treatment on target electrodes in 1M KOH. Solid lines mean the pristine electrodes without treatment, and dot lines indicate APTES treated electrodes.

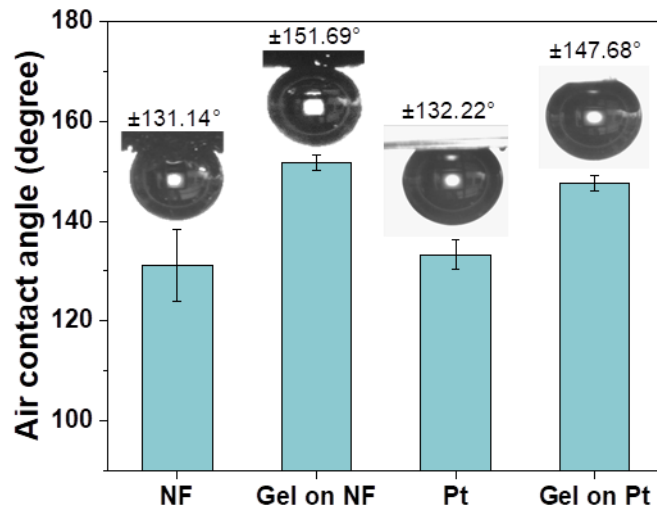


**Figure 10.** The measured air contact angles of PEI 2% aerogels on Ni foam and Pt (FTO). (All the substrates were coated with APTES treatment.)

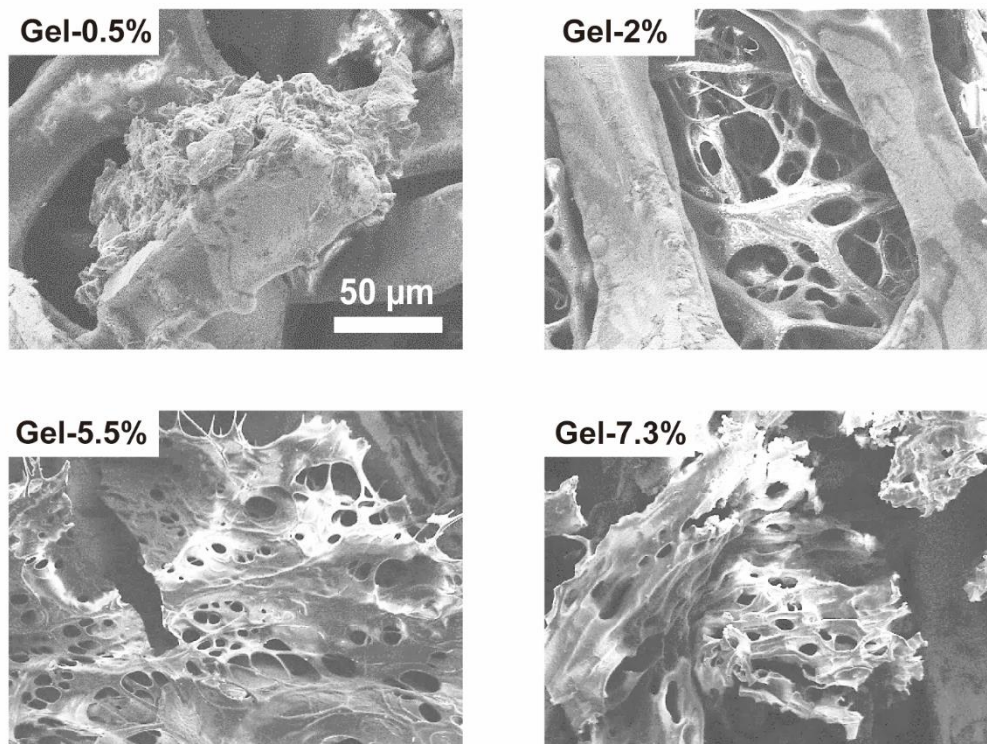


**Figure 11.** SEM images of porous structures with different concentrations of PEI aerogels deposited on Ni foams with APTES treatments.

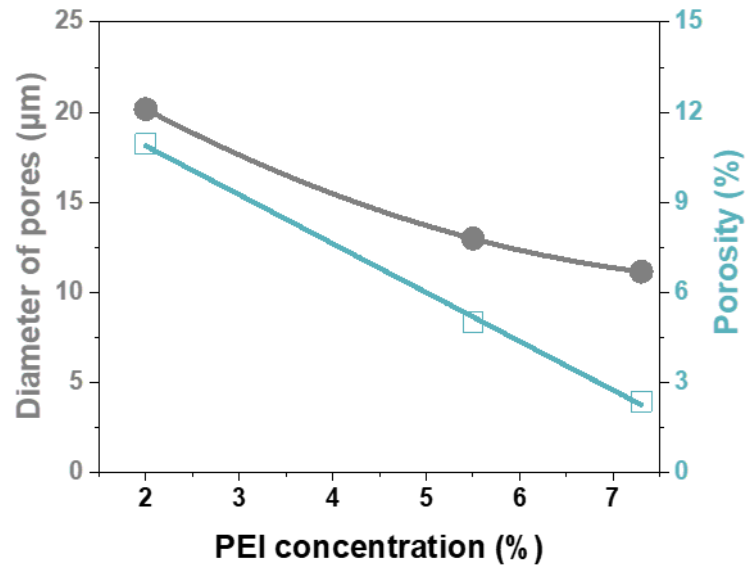


**Figure 12.** The correlations between pore's size and porosity depending on PEI concentrations from Figure 11. (PEI-0.5% didn't form the aerogel, so we excluded it for calculations.)

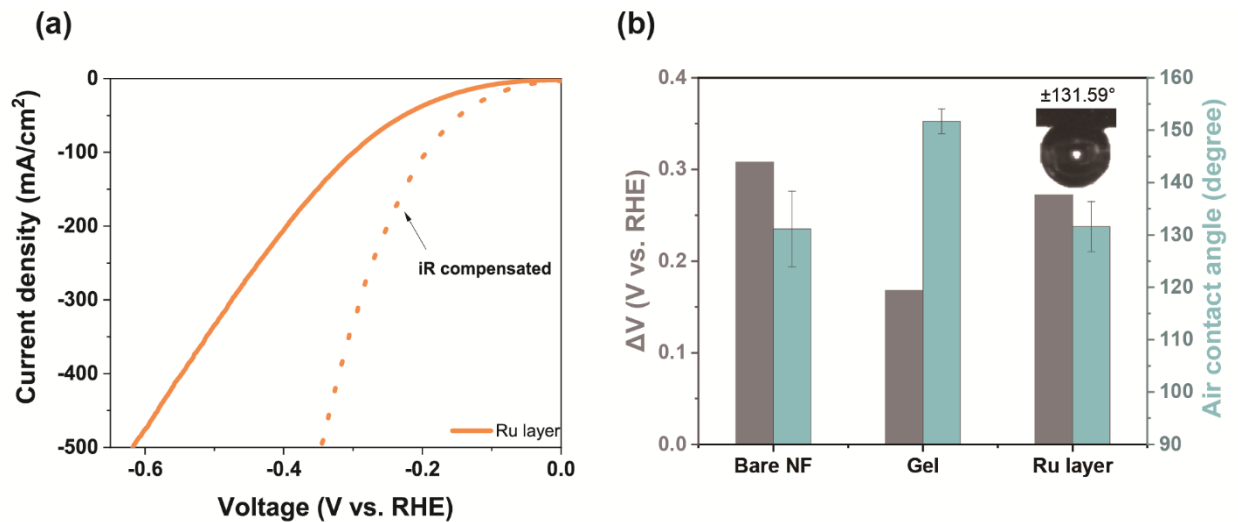


**Figure 13.** (a) The HER effect of Ru layer depending on an iR correction, and (b) the relationship between corresponding discrepancy in applied voltage at  $-500\text{mA}/\text{cm}^2$  (w/ and w/o iR corrections) and air contact angles.

To figure out the HER effect of catalyst-free aerogels in the alkaline media (1M KOH and pH =14), we analyzed the effect of PEI concentrations on superaerophobicity and the structure of the various aerogels (**Figure 7**). First, we measured the HER efficiency of aerogels with different PEI concentrations through a liner sweep voltammetry (LSV) (**Figure 7a**). The applied voltage of bare Ni foam was -0.775 V vs. RHE to reach -500 mA/cm<sup>2</sup>. On the contrary, in the modified system, gel-0.5%, gel-2%, gel-5.5%, gel-7.3% needed -0.656, -0.608, -0.661, and -0.719 V vs. RHE, respectively. Also, we measured air contact angles based on Si wafers to confirm the aerophobicity (**Figure 8**). First, we coated target electrodes with APTES treatment for better adhesion of aerogels, and it had no significant effects on HER (**Figure 9**). The air contact angles of the pristine and APTES-treated Si wafer were 128.69° and 119.28°, respectively. Gel-0.5% showed 131.51° on account of residual hydrophilic PEI. Gel-2%, gel-5.5%, and gel-7.3% had air contact angles of 153.79°, 154.07°, and 147.61°, respectively. Moreover, to affirm the genuine superaerophobicity on target substrates, we coated PEI 2% aerogel on Ni foam and Pt (FTO) based on the result of LSV curves, (a) (**Figure 10**). We observed bare Ni foam and Pt (FTO) had 131.14°, and 132.22°, respectively. Each aerogel deposited electrode was 151.69° on Ni foam and 147.69° on Pt (FTO), and we verified that we realized superaerophobic target substrates with aerogel modifications.

We further investigated the pore structure of aerogels via SEM images (**Figure 11**), and we confirmed that at the lowest concentration of PEI, gel-0.5% cannot form an aerogel due to insufficient PEI concentration to become densely cross-linked. On the other hand, from the concentration of 2% to 7.3%, aerogels were formed, and they had a porous structure within Ni foam skeletons. Additionally, we deduced a correlation of pores' diameters (μm) with porosity (%) of aerogels (**Figure 12**). At the gel-0.5%, it had only Ni foam skeleton with a tiny amount of PEI, we excepted it from the calculations. With increasing PEI concentrations, the following gel-2%, gel-5.5%, and gel-7.3% had the averaged diameter of 20.18 μm, 12.98 μm, 11.15 μm, and the porosity of 0.94, 5.01, 2.37% respectively. Based on these results (**Figure 7b**), we correlated the HER efficiency and aerogel properties (the porosity and air contact angles). Specifically, the air contact angle mostly increased with higher PEI contents, but the pore size and porosity come to decline, and after all, the air contact angle tends to decrease due to lowered swelling behavior ascribed from the excessive aggregation.<sup>31, 32</sup> These suggest that we can induce superaerophobicity of aerogels with a proper porous structure suitable for HER by adjusting the PEI contents.

To verify the efficient HER by aerogels from better wettability, we examined the HER efficiency of PEI 2% aerogels on each target substrate depending on iR corrections (**Figure 7c and 7d**). Since an iR drop is related to the solution resistance in the electrolyte,<sup>33</sup> we speculated the superaerophobic electrodes had relatively low ionic resistance and thus could reduce the discrepancy in the applied voltages between with and without an iR correction. In a porous Ni foam system, we additionally compared the Ru layer as a representative less bubble-repellent catalyst for giving

prominence to the effect of the aerogel. As expected (**Figure 13**), the differences in applied voltages depending on iR corrections (at  $-500 \text{ mA/cm}^2$ ) were 308 mV (Ni foam), 168 mV (aerogel), and 272 mV (Ru layer), respectively. The bubble-repellency notably decreased the difference in applied voltages at high current density. Even in the flat Pt model, the discrepancy (at  $-30 \text{ mA/cm}^2$ ) declined from 234 mV to 202 mV by 13.7%. Moreover, we found that aerogel modifications had no catalytic sites since the LSV curves near onset potentials (bare target substrates and aerogels) were overlapped after iR corrections.

### 3.4 Electrochemical Activities

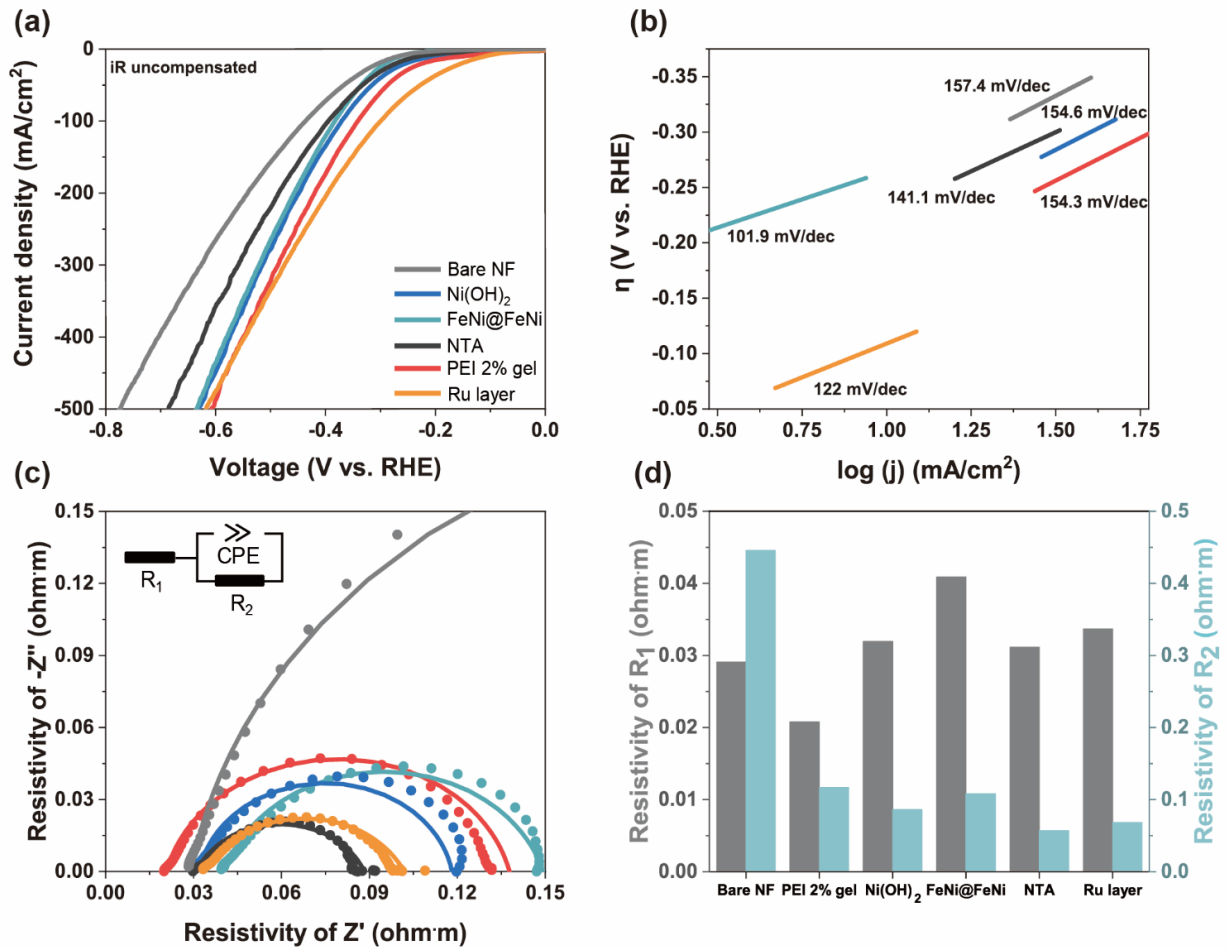


**Figure 14.** (a) The HER performance of PEI 2% aerogel deposited on Ni foam and other electrocatalysts without *i*R corrections. (b) The corresponding Tafel comparison from (a). (c) The EIS analysis of porous Ni foams related to (a). (d) The corresponding bar graph of (c) EIS analysis. (All the target substrates for coating aerogels were pretreated with APTES.)

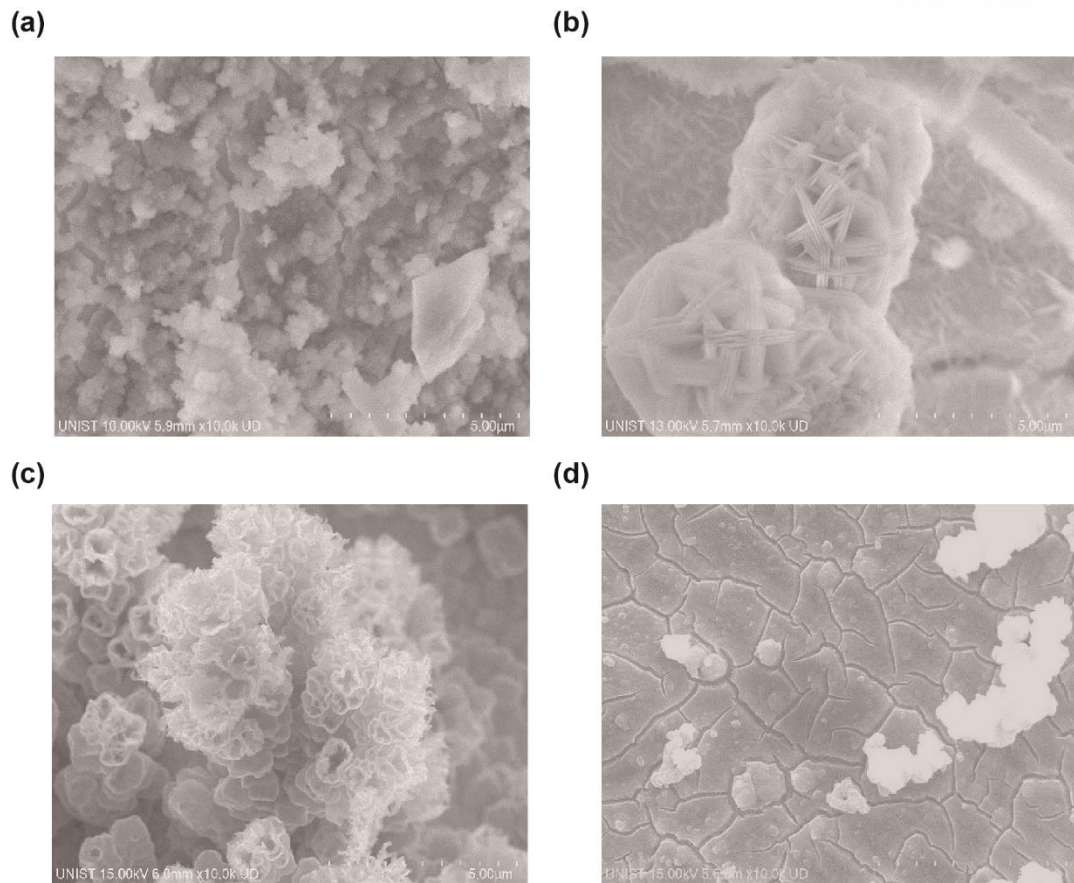


**Figure 15.** SEM images of alkaline electrocatalysts, (a) Ni(OH)<sub>2</sub>, (b) FeNi@FeNi, (c) NTA, and (d) Ru layer.

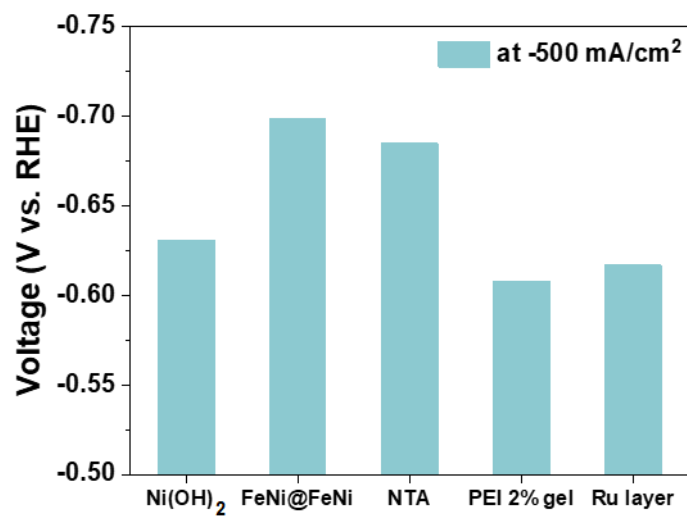


**Figure 16.** The bar graph corresponding to Figure 3a.

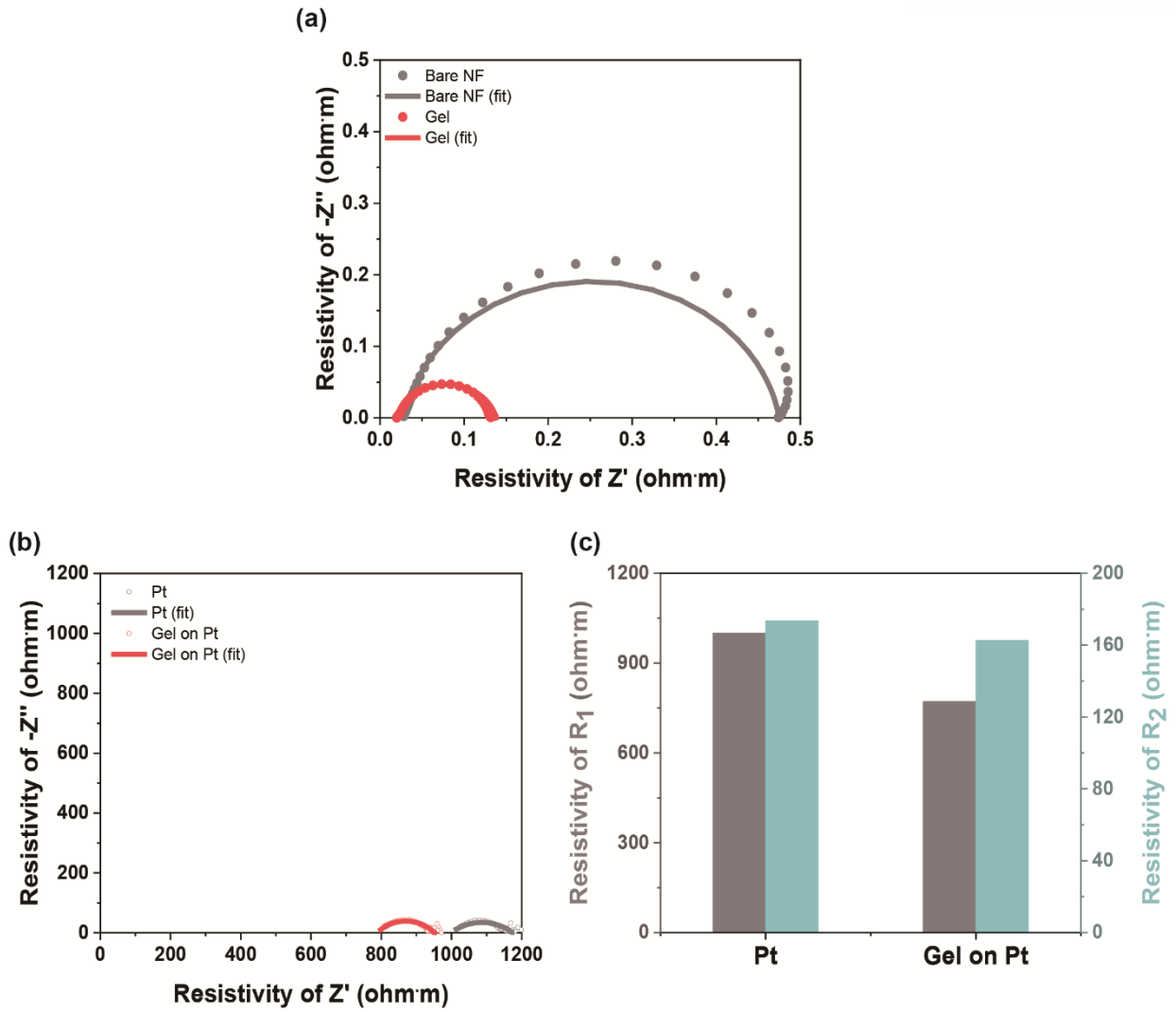


**Figure 17.** (a) The EIS analysis of bare NF and PEI 2% aerogel. (b) The EIS of the flat model and (c) corresponding bare graph.

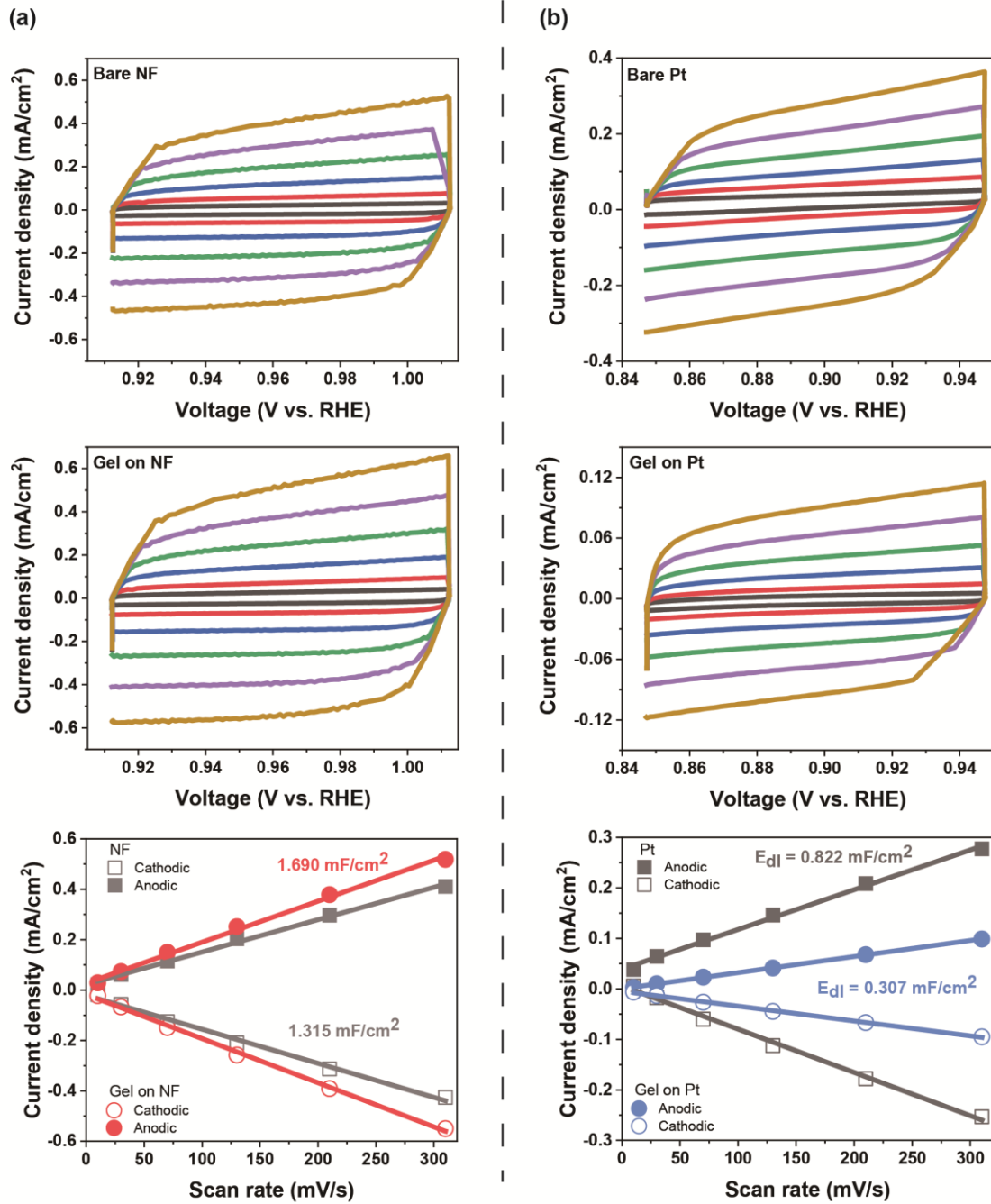


**Figure 18.** (a) The ECSA of bare Ni foam and PEI 2% aerogel on Ni foam. (b) The ECSA of flat Pt model. (Scan rate with 10/30/70/130/210/310 mV/s.)

**Table 1.** The EIS of (a) a porous system and the EIS of (b) a flat system.

(a)

@ -0.25 V vs. RHE	$\rho_1$ [ohm · m]	CPE [F]	$\rho_2$ [ohm · m]
Bare NF	0.0291	0.177e-3 [s <sup>-0.058</sup> ]	0.446
Gel on NF	0.0208	0.254e-3 [s <sup>-0.140</sup> ]	0.117
Ni(OH) <sub>2</sub>	0.0319	0.856e-3 [s <sup>-0.100</sup> ]	0.0862
FeNi@FeNi	0.0409	0.168e-3 [s <sup>-0.167</sup> ]	0.108
NTA	0.0311	0.983e-3 [s <sup>-0.230</sup> ]	0.0571
Ru layer	0.0337	0.939e-3 [s <sup>-0.267</sup> ]	0.0682

(b)

@ -50mA/cm <sup>2</sup>	$\rho_1$ [kohm · m]	CPE [F]	$\rho_2$ [kohm · m]
Bare Pt	0.999	4.71e-3 [s <sup>-0.515</sup> ]	0.174
Gel on Pt	0.771	2.46e-3 [s <sup>-0.446</sup> ]	0.163

To further explore the additional HER effect of the catalyst-free aerogel without iR corrections to mimic the actual HER conditions (**Figure 14**), we compared various alkaline electrocatalyst with the aerogel modification (**Figure 15**). At low current density, the HER performance of the electrocatalyst could be better than the catalyst-free aerogel, but the performance of the aerogel could surpass other electrocatalysts at high current density as a practical water-splitting condition since the superaerophobic aerogel could facilitate dissipation of adhesive bubbles (**Figure 14a** and **16**). From the LSV curves (without iR corrections) (**Figure 14b**), we confirmed the HER mechanism of the aerogel did not significantly change based on the almost same Tafel slope with pristine. This implies the identical tendency with the LSV data depending on iR corrections.

In this regard, we supplementally conducted electrochemical impedance spectroscopy (EIS) (**Figure 14c, 14d, 17, and Table 1**) and measured double-layer capacitance values to support the better wettability of aerogel modifications. In EIS analysis, we plotted EIS based on the resistivity ( $\rho$ ) (ohm·m) so that we intentionally eliminated the deviation of the impedance caused by each surface area. In the porous model (Ni foam), the resistivity was measured near the onset potential of aerogels (-0.25 V vs. RHE). The  $\rho_1$  from the series resistance related to the solution resistance by the ionic conductance, of PEI 2% aerogel had the lowest value than pristine and other electrocatalysts. Whereas the  $\rho_2$  resulting

from charge-transfer resistance, of PEI 2% aerogel has been dramatically decreased than bare Ni foam, but slightly greater than other alkaline catalysts. The equivalent tendency was predominant in Pt (FTO) measured at  $-50 \text{ mA/cm}^2$ . The  $\rho_2$  decreased by 6.3% after the deposition of the layer, on the other hand, the  $\rho_1$  greatly decreased by 23% from the pristine.

According to **Figure 18**, the double-layer capacitance values of Ni foam and PEI aerogel were 1.315, and 1.690  $\text{mF/cm}^2$ , respectively. Electrochemical surface areas of a porous system have been kept in similar. On the contrary, on the flat Pt (FTO), the double-layer capacitance values decreased from 0.822 to 0.307  $\text{mF/cm}^2$  due to the direct shielding of the Pt film by the insulated aerogel layer. Combined with EIS analysis, the HER performance of aerogel modification comparable to other electrocatalysts in the porous model and the HER performance surpassed Pt in the flat model were linked to the notably declined solution resistance through the electrolyte and electrode due to easy elimination of adhered hydrogel bubbles. These results follow the  $iR$  corrections to elucidate the superaerophobicity underlying each substrate.

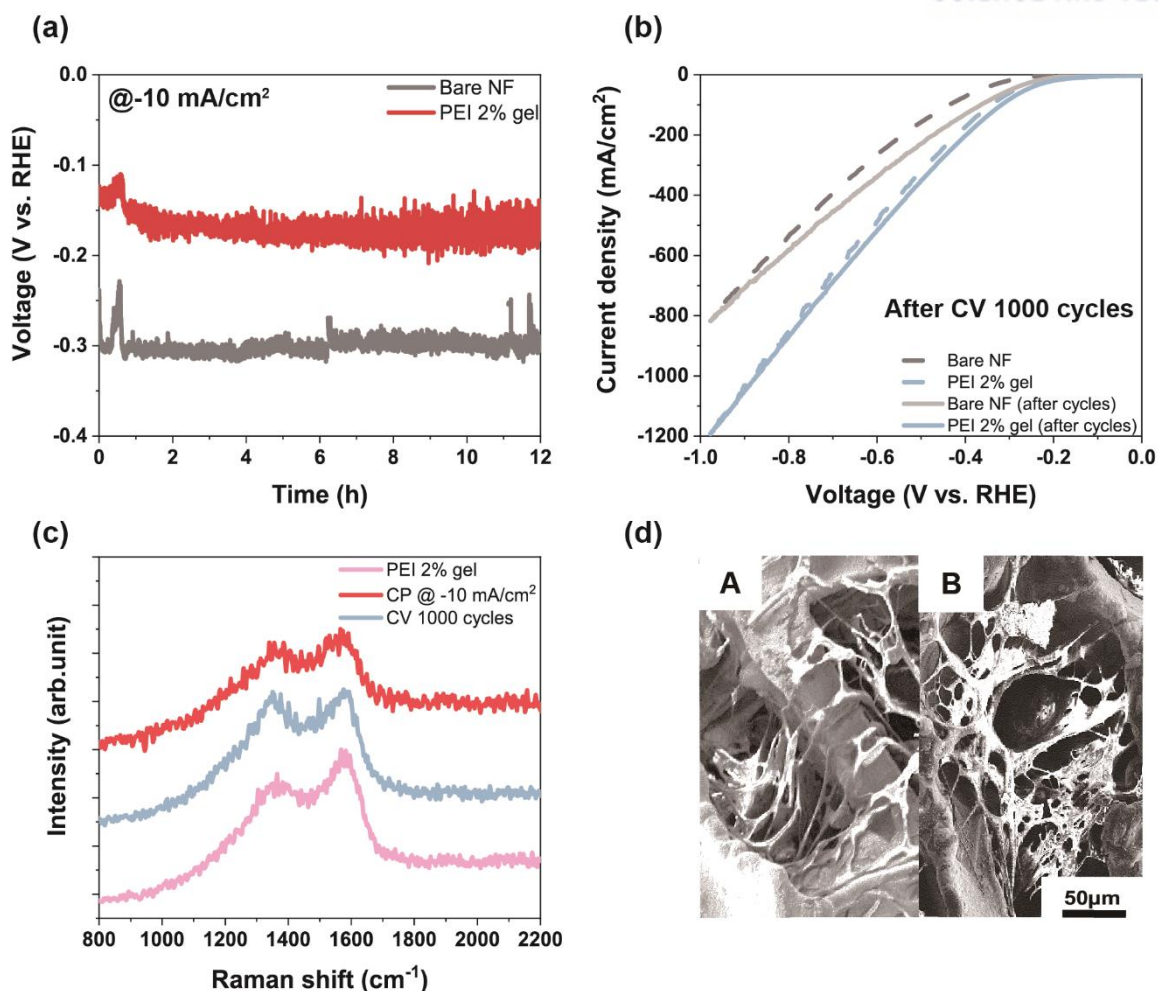


**Figure 19.** (a) Chronopotentiometry at  $-10 \text{ mA/cm}^2$  for 12hr with 350 rpm of the aerogel deposited on Ni foam vs. bare Ni foam. (b) Measurement of LSV after the cyclic voltammetry (CV) 1000 times within the same sweep potential range. (c) Raman shift to confirm the functional groups after long-term stability tests. (d) SEM images after A: (a)/B: (b) stability tests, respectively.

To confirm the stability of the aerogel modification (**Figure 19**), we conducted two types of long-term stability tests. In a chronopotentiometry at  $-10 \text{ mA/cm}^2$  (**Figure 19a**), PEI 2% aerogel remained its applied potential at around  $-0.2 \text{ V vs. RHE}$ , while bare Ni foam showed about  $-0.3 \text{ V vs. RHE}$  for 12 hours. After repeating cyclic voltammetry 1000 times with a scan rate of  $100 \text{ mV/s}$  (took more than 7 hours) (**Figure 19b**), both bare Ni foam and PEI 2% aerogel had almost kept in constant with initial LSV curves. Also, to ascertain the aerogel structure after the long-term electrochemical tests, we examined Raman spectroscopy at  $532 \text{ nm}^{-1}$  and scanning electron microscopy (SEM) (**Figure 19c** and **19d**). In Raman spectroscopy, the two obvious peaks of the aerogels deposited on Ni foams have been maintained at  $1364 \text{ cm}^{-1}$  and  $1573 \text{ cm}^{-1}$  before and after the tests. The followings are  $\text{CH}_2$  wagging and  $\text{NH}_2$  with different degrees of protonation by interacting with metal, respectively.<sup>34-37</sup> Moreover, we verified that pore structures of aerogels have been almost identical before and after the tests by SEM.

## Conclusion

In summary, the catalyst-free PEI aerogel modified system provided a simple strategy to enhance HER in the aspect of practical bubble detachment. Using PEI as a building block with 1wt% GA as a cross-linker, we could control the pore structure of PEI aerogel and realize the superaerophobic electrodes. The aerogel could facilitate the as-generated bubble detachment on the surface of the electrode during HER, and it had the HER performance comparable to other electrocatalysts. Moreover, in flat Pt (FTO), the overall HER efficiency of the aerogel layer deposited on Pt surpassed flat Pt films. Our results suggest that cheap-based polymer aerogels can deal the impeded mass transfer due to adhered gas bubbles for designing the energy conversion devices such as an electrolyzer.

## References

1. Zhao, G.; Rui, K.; Dou, S. X.; Sun, W., Heterostructures for Electrochemical Hydrogen Evolution Reaction: A Review. *Adv. Funct. Mater.* **2018**, *28* (43), 1803291.
2. Daiyan, R.; MacGill, I.; Amal, R., Opportunities and Challenges for Renewable Power-to-X. *ACS Energy Lett.* **2020**, *5* (12), 3843-3847.
3. Zhu., J.; Hu., L.; Zhao., P.; Lee., L. Y. S.; Wong., K.-Y., Recent Advances in Electrocatalytic Hydrogen Evolution Using Nanoparticles. *Chem. Rev.* **2020**, *120* (2), 851-918.
4. Lu, Z.; Li, Y.; Lei, X.; Liu, J.; Sun, X., Nanoarray based "superaerophobic" surfaces for gas evolution reaction electrodes. *Mater. Horiz.* **2015**, *2* (3), 294-298.
5. Lu, Z.; Zhu, W.; Yu, X.; Zhang, H.; Li, Y.; Sun, X.; Wang, X.; Wang, H.; Wang, J.; Luo, J.; Lei, X.; Jiang, L., Ultrahigh Hydrogen Evolution Performance of Under-Water "Superaerophobic" MoS<sub>2</sub> Nanostructured Electrodes. *Adv. Mater* **2014**, *26* (17), 2683-2687.
6. Jiang., M.; Wang., H.; Li., Y.; Zhang., H.; Zhang., G.; Lu., Z.; Sun., X.; Jiang., L., Superaerophobic RuO<sub>2</sub> -Based Nanostructured Electrode for High-Performance Chlorine Evolution Reaction. *Small* **2017**, *13* (4), 1602240.
7. Kim., B. K.; Kim., M. J.; Kim., J. J., Impact of Surface Hydrophilicity on Electrochemical Water Splitting. *ACS Appl. Mater. Interfaces* **2021**, *13* (10), 11940-11947.
8. Song, Q.; Xue, Z.; Liu, C.; Qiao, X.; Liu, L.; Huang, C.; Liu, K.; Li, X.; Lu, Z.; Wang, T. A., General Strategy to Optimize Gas Evolution Reaction via Assembled Striped-Pattern Superlattices. *J. Am. Chem. Soc.* **2020**, *142* (4), 1857-1863.
9. Angulo., A.; Linde., P. v. d.; Gardeniers., H.; Modestino., M.; Rivas, D. F., Influence of Bubbles on the Energy Conversion Efficiency of Electrochemical Reactors. *Joule* **2020**, *4* (3), 555-579.
10. Zhang., L.; Huang., J.; Zheng., Q.; Li., A.; Li., X.; Li., J.; Shao., M.; Chen., H.; Wei., Z.; Deng., Z.; Li., C., "Superaerophobic" NiCo bimetallic phosphides for highly efficient hydrogen evolution reaction electrocatalysts. *Chem. Commun.* **2021**, *57* (50), 6173-6176.
11. Kim., Y. J.; Lim., A.; Kim., J. M.; Lim., D.; Chae., K. H.; Cho., E. N.; Han., H. J.; Jeon., K. U.; Kim., M.; Lee., G. H.; Lee., G. R.; Ahn., H. S.; Park., H. S.; Kim., H.; Kim., J. Y.; Jung., Y. S., Highly efficient oxygen evolution reaction via facile bubble transport realized by three-dimensionally stack-printed catalysts. *Nat. Commun.* **2020**, *11*, 4921.
12. Law., K.-Y., Definitions for Hydrophilicity, Hydrophobicity, and Superhydrophobicity: Getting the Basics Right. *J. Phys. Chem. Lett.* **2014**, *5* (4), 686-688.
13. Tan., Y.; Yin., Y.; Yin., X.; Lan., C.; Wang., Y.; Hu., F.; Huang., Q.; Mi., Y., A "Superaerophobic" Se-Doped CoS<sub>2</sub> Porous Nanowires Array for Cost-Saving Hydrogen Evolution. *Catalysts* **2021**, *11* (2), 169.

14. Li., H.; Chen., S.; Zhang., Y.; Zhang., Q.; Jia., X.; Qi Zhang, L. G.; Sun., X.; Song., L.; Wang., X., Systematic design of superaerophobic nanotube-array electrode comprised of transition-metal sulfides for overall water splitting. *Nat. Commun.* **2018**, *9*, 2452.
15. George, J. E.; Chidangil, S.; George, S. D., Recent Progress in Fabricating Superaerophobic and Superaerophilic Surfaces. *Adv. Mater. Interfaces* **2017**, *4* (9), 1601088-160123.
16. Cao, Z.; Stevens, M. J.; Carrillo, J. M.; Dobrynin, A. V., Adhesion and Wetting of Soft Nanoparticles on Textured Surfaces: Transition between Wenzel and Cassie-Baxter states. *Langmuir* **2015**, *31* (5), 1693-1703.
17. Wang., J.; Li., T.; Li., Y.; Duan., Y.; Jiang., Y.; Arandiyani., H.; Li., H., Wetting Transitions of Liquid Gallium Film on Nanopillar-Decorated Graphene Surfaces. *Molecules* **2018**, *23* (10), 2407.
18. Jeon., D.; Park., J.; Shin., C.; Kim., H.; Jang., J.-W.; Lee., D.; Ryu., J., Superaerophobic hydrogels for enhanced electrochemical and photoelectrochemical hydrogen production. *Sci. Adv.* **2020**, *6*.
19. Mani, N. K.; Rudiuk, S.; Baigl, D., Spatially controlled DNA unzipping by microfluidic interface positioning on a molecule perpendicular to a multicomponent flow. *Chem. Commun* **2013**, *49* (61), 6858-6860.
20. Davidson-Hall, T.; Aziz, H., The role of polyethylenimine in enhancing the efficiency of quantum dot light-emitting devices. *Nanoscale* **2018**, *10* (5), 2623-2631.
21. Ohisa., S.; Takashima., D.; Chiba., T.; Kido., J., Low-temperature cross-linking of polyethyleneimine ethoxylated using silane coupling agents to obtain stable electron injection layers in solution-processed organic light-emitting devices. *J. Mater. Chem. C* **2019**, *7* (22), 6759-6766.
22. Zhang., B.; Liu., J.; Wang., J.; Ruan., Y.; Ji., X.; Xu., K.; Chen., C.; Wan., H.; Miao., L.; Jiang., J., Interface engineering: The Ni(OH)<sub>2</sub> /MoS<sub>2</sub> heterostructure for highly efficient alkaline hydrogen evolution. *Nano Energy* **2017**, *37*, 74-80.
23. Huang., K.; Dong., R.; Wang., C.; Li., W.; Sun., H.; Geng., B., Fe–Ni Layered Double Hydroxide Arrays with Homogeneous Heterostructure as Efficient Electrocatalysts for Overall Water Splitting. *ACS Sustain. Chem. Eng.* **2019**, *7* (17), 15073-15079.
24. Li., D.; Hao., G.; Guo., W.; G. Liu, J. L.; Zhao., Q., Highly efficient Ni nanotube arrays and Ni nanotube arrays coupled with NiFe layered-double-hydroxide electrocatalysts for overall water splitting. *J. Power Sources* **2020**, *448*, 227434.
25. Xia., J. W.; Volokh., M.; Peng., G. M.; Fu., Y. S.; Wang., X.; Shalom., M., Low-Cost Porous Ruthenium Layer Deposited on Nickel Foam as a Highly Active Universal-pH Electrocatalyst for the Hydrogen Evolution Reaction. *ChemSusChem* **2019**, *12*, 2780-2787.

26. Virgen-Ortíz., J. J.; Santos., J. C. S. d.; Berenguer-Murcia., Á.; Barbosa., O.; Rodrigues.; Fernandez-Lafuente., R., Polyethylenimine: a very useful ionic polymer in the design of immobilized enzyme biocatalysts. *J. Mater. Chem. B* **2017**, *5* (36), 7461-7490.
27. Lindén., J. B.; Larsson., M.; Kaur., S.; Nosrati., A.; Nydén., M., Glutaraldehyde-crosslinking for improved copper absorption selectivity and chemical stability of polyethyleneimine coatings. *J. Appl. Polym. Sci.* **2016**, *133* (37), 43954.
28. Hwang., K.-S.; Park., H.-Y.; Kim., J.-H.; Lee., J.-Y., Fully organic CO<sub>2</sub> absorbent obtained by a Schiff base reaction between branched poly(ethyleneimine) and glutaraldehyde. *Korean J. Chem. Eng.* **2018**, *35* (3), 798-804.
29. Movahedi, A.; Lundin, A.; Kann, N.; Nyden, M.; Moth-Poulsen, K., Cu(I) stabilizing crosslinked polyethyleneimine. *Phys. Chem. Chem. Phys.* **2015**, *17* (28), 18327-18336.
30. Linden, J. B.; Larsson, M.; Kaur, S.; Skinner, W. M.; Miklavcic, S. J.; Nann, T.; Kempson, I. M.; Nyden, M., Polyethyleneimine for copper absorption II: kinetics, selectivity and efficiency from seawater. *RSC Adv.* **2015**, *5* (64), 51883-51890.
31. Hong, P. D.; Chou, C. M.; He, C. H., Solvent effects on aggregation behavior of polyvinyl alcohol solutions. *Polymer* **2001**, *42* (14), 6105-6112.
32. Gambinossi., F.; Ferri., J., Effect of electrolyte-induced polymer swelling on macromolecule functionalized core-shell nanoparticle interaction potential: Calculation of colloidal stability ratio. *Colloids Surf., A* **2015**, *464*, 143-153.
33. Lindsay., F. G.; Taylor., R. J., iR correction: Part I. A computerised interrupt method. *J. Electroanal. Chem.* **1980**, *108* (3), 293-303.
34. Sanchez-Cortes, S.; Berenguel, R. M.; Madejon, A.; Perez-Mendez, M., Adsorption of polyethyleneimine on silver nanoparticles and its interaction with a plasmid DNA: a surface-enhanced Raman scattering study. *Biomacromolecules* **2002**, *3* (4), 655-660.
35. Hu, Z.; Wang, X.; Wang, W.; Zhang, Z.; Gao, H.; Mao, Y., Raman spectroscopy for detecting supported planar lipid bilayers composed of ganglioside-GM1/sphingomyelin/cholesterol in the presence of amyloid-beta. *Phys. Chem. Chem. Phys.* **2015**, *17* (35), 22711-22720.
36. Huang, X.; Ishitobi, H.; Inouye, Y., Formation of fluorescent platinum nanoclusters using hyper-branched polyethylenimine and their conjugation to antibodies for bio-imaging. *RSC Adv.* **2016**, *6* (12), 9709-9716.
37. Lee., K.; Lee., J.; Kwon., K. W.; Park., M.-S.; Hwang., J.-H.; Kim., K. J., 3D Graphene-Ni Foam as an Advanced Electrode for High-Performance Nonaqueous Redox Flow Batteries. *ACS Appl. Mater. Interfaces* **2017**, *9* (27), 22502-22508.

## Acknowledgements

벌써 유니스트에서 공부한 지, 6 년이 지났습니다. 힘든 순간들도 많았지만, 추억이 되는 순간들도 많았던 것 같습니다. 어제 무엇을 먹었는지조차 가물가물한 저에게, 석사 논문이라는 인생에서 중요한 기록을 남기니, 유니스트에서의 기억이 주마등처럼 스쳐 지나가는 것 같습니다.

어렸을 때는 터무니없는 꿈도 꾸면서 어른이 되면 어떤 사람이 될지 궁금했는데, 막상 어른이 되어보니 그저 과제와 치열한 일상생활을 견디는 존재가 되었습니다. 대학교를 졸업하고, 진짜 내가 어떤 사회 구성원으로 성장할지 고민하며 대학원에 진학하였고, 어쩌면 대학생활 동안의 그 어떤 전공 공부보다 석사 기간이 가장 재미있고 값진 경험이었던 것 같습니다. 제 인생을 한 층 성장할 수 있도록 좋은 연구 기회를 주신 류정기 교수님께 감사드립니다. 또한, 저의 석사 논문 심사를 맡아 주신 이동욱 교수님, 장지욱 교수님께 정말 감사드립니다. 그리고 연구에 대한 조언을 아낌없이 해준 화목한 우리 BFML 구성원들에게도 감사합니다.

또한, 저의 지치는 일상의 활력소가 되어준 친구들에게 너무 고맙습니다. 공감대를 이루고 서로 대화를 나눌 수 있는 존재가 있다는 사실이 모든 힘든 순간을 극복할 수 있는 원동력이었던 것 같습니다.

마지막으로, 항상 바쁘다고 연락도 자주 안 하고 집도 못 간 딸을 항상 걱정해 주신 부모님께 죄송하기도 하고 정말 고맙습니다. 학교라는 보호막을 벗어나, 진짜 사회로 나가는 만큼 부모님의 더욱더 그리울 것 같습니다.

